High-spin level scheme of ¹⁹⁴Pb

T. Kutsarova, E. A. Stefanova,[*] and A. Minkova

Institute for Nuclear Research and Nuclear Energy, BAS, BG-1784 Sofia, Bulgaria

S. Lalkovski[†]

Faculty of Physics, University of Sofia "St. Kliment Ohridski," BG-1164 Sofia, Bulgaria

A. Korichi, A. Lopez-Martens, and F. Hannachi[‡]

CSNSM Orsay, IN2P3/CNRS, F-91405, France

H. Hübel

HISKP, Helmholtz-Institute für Strahlen-und Kernphysik, Nussallee 14-16, D-53115, Germany

A. Görgen,[§] A. Jansen, and G. Schönwasser

ISKP, Universität Bonn, Nussallee 14-16, D-53115, Germany

T. L. Khoo

Physics Division, Argonne National Laboratory, Argonne, Illinois 60439, USA

B. Herskind and M. Bergström

The Niels Bohr Institute, Blegdamsvej 17, DK-2100 Copenhagen, Denmark

D. Bazzacco

Dipartimento di Fisica, Universitá di Padova and INFN Sezione di Padova, I-35131 Padova, Italy

Z. Podolyák[‖]

INFN, Laboratori Nazionali di Legnaro, Italy

High-spin states in ¹⁹⁴Pb have been populated in the ¹⁶⁸Er(³⁰Si,4n) reaction at 142 MeV. The emitted γ rays were detected by the EUROBALL III multidetector array. The level scheme was considerably extended and many previously observed γ-ray transitions were reordered. Four new magnetic rotational bands were observed. The energies and spins of the bandheads of all previously observed magnetic rotational bands were corrected based on the observation of new transitions. From nine observed bands, only one could not be connected to the lower lying states. Based on comparison systematics with neighboring Pb isotopes and tilted-axis cranking model calculations previously reported, configuration assignments to the observed bands have been made.

I. INTRODUCTION

The nuclear spectra of the neutron-deficient lead nuclei are rich on coexisting nuclear excitations. Because of the closed proton shell at $Z = 82$ their ground state is known to have a spherical shape and the low-lying yrast states are mainly of a two-quasiparticle neutron configuration. Together with the spherical minimum, prolate and oblate minima at low energies have been predicted theoretically [1] for the light Pb nuclei. Both superdeformed prolate and weakly deformed oblate excitations are observed in the light Pb isotopes, in particular in ¹⁹⁴Pb [2–7]. The origin of the oblate states is connected with proton excitations across the gap to the deformation driving $h_{9/2}$ and $i_{13/2}$ orbitals. The structures built directly on such oblate states, however, do not correspond to the expected rotational bands but resemble the spherical multiplet-like pattern. In competition with these excitations, regular cascades of strongly enhanced $M1$ transitions were observed in Pb isotopes some years ago [8] and have been studied extensively. As a result, a new mechanism of nuclear excitations—named magnetic rotation—has been established. Its description has been provided by the tilted-axis cranking (TAC) model of Frauendorf [9]. The magnetic rotational bands result from the

———————

[*]Present address: Physics Department, TSU, Houston, TX 77004, USA.

[†]Present address: School of Environment and Technology, University of Brighton, Brighton BN2 4GJ, UK.

[‡]Present address: Centre d'Etudes Nuclaires de Bordeaux-Gradignan, Gradignan, France.

[§]Present address: DAPNIA/SPhN, CEA-Saclay, Gif-sur-Yvette, France.

[‖]Present address: Department of Physics, University of Surrey, Guildford, GU2 7XH, UK.

coupling of the angular momentum vectors of high-j proton particles and high-j neutron holes outside a spherical core. Angular momentum and excitation energy along the bands are increased by a step-by-step alignment of proton and neutron spins in the direction of the total angular momentum. Since this resembles the closing of a pair of shears, the $M1$ bands have also been called "shears bands" [8]. With the increasing spin the values of the reduced transition probabilities $B(M1)$ gradually decrease, as confirmed by lifetime measurements (see, e.g., Ref. [10] and references therein). The enhanced $M1$ transitions are due to the rotation of the magnetic dipoles around the total angular momentum [11]. In addition to the TAC model [9], these bands have been reproduced in terms of an effective interaction between the proton and neutron spins by Macchiavelli *et al.* [12–15].

After the discovery of magnetic bands in ^{199,200}Pb [8], the neighboring Pb isotopes attracted many studies [16,17]. Nevertheless, the level schemes of most of the nuclei are incomplete with bands not connected to the lower lying levels. The detailed study of ^{196}Pb [18], where a total of nine bands were observed with comprehensive connections to the normal states and other bands, is an exception. Before the present work, the most complete high-spin study of ^{194}Pb was done by Kaci *et al.* [19]. Many interband connections were suggested, but not seen. The aim of the present work is to expand the level scheme similar to that of ^{196}Pb [18] to allow for more detailed systematic study between the two nuclei and in the region.

II. EXPERIMENT AND ANALYSIS

Excited states in ^{194}Pb were populated by the ^{30}Si + ^{168}Er reaction at a beam energy of 142 MeV. The beam was provided by the XTU tandem accelerator at the Legnaro National Laboratory. The target consisted of 1.15 mg/cm^2 of ^{168}Er deposited on a 9 mg/cm^2 gold backing to slow down and finally stop the recoiling nuclei. The prompt γ rays emitted from the excited nuclei were detected by the EUROBALL III multidetector array [20], consisting of 30 single HPGe Compton-shielded detectors, 26 Clover, and 15 Cluster composite Compton-shielded detectors. Events were collected with the requirement that at least five unsuppressed Ge detectors fired in coincidence. We recorded about 2×10^9 triple and higher fold coincidence events. In the off-line analysis the Compton-suppressed events were unpacked into triple coincidences and sorted into two three-dimensional E_γ-E_γ-E_γ arrays using the RADWARE package [21]. One of the cubes was up to energy of 4 MeV; the other one extended from very low energies up to 1 MeV. Gamma-ray coincidence spectra were then obtained by setting double gates in the E_γ-E_γ-E_γ cubes. Furthermore, spectra gated by two transitions in ^{194}Pb were built at 15.45°, 34.60°, 52.23°, 76.54°, 103.19°, 129.57°, 137.20°, and 156.22° detection angles of Euroball III to analyze angular distributions. The γ intensities of the transitions were determined from several multigated spectra obtained as a sum of the individual spectra of the Ge detectors, by applying appropriate intensity normalization.

III. EXPERIMENTAL RESULTS

The positive-parity and the negative-parity parts of the level scheme of ^{194}Pb obtained in the present work are displayed in Fig. 2 (Parts A–C) and Fig. 2 (Parts E and F), respectively. The level scheme is based on triple coincidence relationships, the transition intensities, and angular distribution results for a number of the new transitions. As can be seen from Figs. 2 and 2 the level scheme is very complex. Several transitions connecting mainly groups 2 and 6 are not shown in Fig. 2 and can be found in Table I. Previous to our work the level scheme has been studied by several groups [19,22–24]. The most complete level scheme was published by Kaci *et al.* [19]. In the following we shall refer mainly to this work. The present level scheme of ^{194}Pb is extended with respect to that of Ref. [19]. We observed four new weak sequences of low-energy transitions and found links from the low- and high-spin parts of certain bands to the spherical states, which allowed us to correct the excitation energies and spins of the bandheads of all bands. We also extended considerably the normal part of the level scheme. About 180 new transitions were observed and placed in the level scheme. These data are summarized in Table I. The total population of the nucleus ^{194}Pb in the reaction is distributed between the prompt feeding into the yrast levels and the direct population of the 11^- and 12^+ isomeric states [19]. Our data show the same relative population as in Ref. [19]; however, the fraction feeding the 12^+ state is redistributed to account for about 8% of the intensity of the 1215.6-keV transition. The intensity of the weaker transitions populating the 12^+ isomer has been estimated to be less than 3% of the total population of ^{194}Pb. These results are used for intensity normalization (see Table I).

A. Positive-parity bands

1. Band 1

Band 1 (presently shown in Fig. 2, Part A) is reported in Ref. [19] as band 2a below and band 2b above the band crossing. The bandhead was positioned at the 4376-keV level with spin and parity 13^+ [19]. The energy of another level at 4643 keV was fixed by its decay (transitions 1082, 507 keV) to the strongest sequence of the spherical levels built on the 12^+ isomer at 2628.1 keV. Between these levels two $M1$ transitions of 130 and 137 keV were placed as the $14^+ \rightarrow 13^+$ and $15^+ \rightarrow 14^+$ members of band 2a, respectively [19]. In the present work, coincidences between the 1215.6–668.4–130.2-keV cascade of group 1 and the transitions of band 1 except for the 137.0-keV one were observed. These coincidences suggest an existence of a new level at an energy of 4512.1 keV and a reordering of the 130.2- and 137.0-keV transitions. Two new low-energy transitions of 138.9 and 128.3 keV showing coincidences with the transitions of band 1 could be resolved and placed parallel to the 130.2–137.0-keV cascade in an unique arrangement owing to the coincidences of 138.9 keV with the new sequence of group 1 (567.7–586.9–767.8 keV) and with the structure built on the 11^- isomer via the 664.9-keV transition. Furthermore, we found linking transitions from the upper part of band 1 to the spherical states of group 1 built on the 12^+ isomer, which required

TABLE I. Energies, intensities, angular distribution coefficients, multipolarities, and level assignments (angular momentum and energy) for transitions in ^{194}Pb observed in the present work.

$E_\gamma{}^{a}$ (keV)	I_γ	I_{tot}	a_2	Multipolarity	J_i^π	J_f^π	E_i (keV)
Band 1							
58.3					(16^+)	15^+	4700.9
65.5					17^+	(16^+)	4766.4
163.0	39(6)	133		$M1$	18^+	17^+	4929.4
212.3	21(5)	45		$M1$	24^+	23^+	6841.9
227.6	19(4)	37		$M1$	25^+	24^+	7069.5
260.7	28(6)	47		$M1$	23^+	22^+	6629.6
266.8	15(3)	24		$M1$	26^+	25^+	7336.3
303.0	89(14)	127		$M1$	19^+	18^+	5232.4
306.9	13(3)	20		$M1$	27^+	26^+	7643.2
360.8	9.3(30)	12		$M1$	28^+	27^+	8004.0
363.4	40(7)	50		$M1$	22^+	21^+	6368.9
376.3	67(9)	83		$M1$	21^+	20^+	6005.5
394.1	6.7(20)	8.1		$M1$	29^+	28^+	8398.1
396.8	90(13)	109		$M1$	20^+	19^+	5629.2
420.9	3.8(13)	4.4		$(M1)$	(30^+)	29^+	8819.0
441	2.3(10)	2.7		$(M1)$	(31^+)	(30^+)	9260
462	1.6(8)	1.8		$(M1)$	(32^+)	(31^+)	9722
484	1.1(5)	1.2		$(M1)$	(33^+)	(32^+)	10206
624.1	2.0(9)	2.0		$E2$	23^+	21^+	6629.6
699.8	5.5(17)	5.5		$E2$	20^+	18^+	5629.2
739.7	7.7(23)	7.8		$E2$	22^+	20^+	6368.9
773.1	13(4)	14		$E2$	21^+	19^+	6005.5
Decay of Band 1							
128.3			$-0.24(7)$	$M1$	14^+	13^+	4503.4
130.2			$-0.20(7)$	$M1$	15^+	14^+	4642.3
137.0			$-0.14(7)$	$M1$	14^+	13^+	4512.1
138.9				$M1$	15^+	14^+	4642.3
248.3	2.4(9)	4.1		$M1$	(16^+)	15^+	4701.0
255.9	1.3(5)	2.1		$M1$	23^+	22^+	6629.6
286.4	0.7(3)	1.0	$-0.3(2)$	$M1$	22^+	21^+	6368.9
507.1	5.2(16)	5.8		$M1$	15^+	16^+	4642.3
819.6	4.7(15)	4.7	$0.4(1)$	$E2$	22^+	20^+	6368.9
1081.8	1.9(9)	2.0		$M1$	15^+	14^+	4642.3
Band 1a							
347.9	20(4)	26		$M1$	23^+	22^+	6762.7
351.5	13(4)	17		$M1$	24^+	23^+	7114.2
317.3	4.9(15)	6.8		$M1$	25^+	24^+	7431.5
Decay of Band 1a							
409.3	25(5)	30		$M1$	22^+	21^+	6414.8
785.6	5.8(18)	5.9		$E2$	22^+	20^+	6414.8
Band 1b							
268.8	6.2(20)	10		$(M1)$	(24^+)	23^+	7067.4
296.4	6.2(18)	9.0		$(M1)$	(25^+)	(24^+)	7363.8
315.5	5.8(18)	8.1		$(M1)$	(26^+)	(25^+)	7679.3
331.6	2.0(8)	2.7		$(M1)$	(28^+)	(27^+)	8352.9
342.0	3.1(12)	4.1		$(M1)$	(27^+)	(26^+)	8021.3
Decay of Band 1b							
304.7	3.0(12)	4.3		$(M1)$	(24^+)	23^+	7067.4
383.8	4.9(15)	6.0	$-0.3(1)$	$M1$	23^+	22^+	6798.6
793.1	4.3(13)	4.3		$E2$	23^+	21^+	6898.6
Band 2							
$(85)^{b}$				$(M1)$	16^+	(15^+)	4725.7
162.6	7.8(22)	27		$M1$	17^+	16^+	4888.3

TABLE I. *(Continued.)*

E_γ[a] (keV)	I_γ	I_{tot}	a_2	Multipolarity	J_i^π	J_f^π	E_i (keV)
232.8	17(4)	33		$M1$	18^+	17^+	5121.1
288.1	22(4)	33		$M1$	19^+	18^+	5409.2
347.6	17(3)	23		$M1$	20^+	19^+	5756.8
361.0	1.6(8)	2.1		$(M1)$	(25^+)	(24^+)	7637.5
371.5	2.4(10)	3.0		$(M1)$	(24^+)	(23^+)	7276.5
374.2	11(3)	14		$M1$	21^+	20^+	6131.0
377.2	3.2(7)	3.9		$(M1)$	(23^+)	22^+	6905.0
396.8	7.2(17)	8.7		$M1$	22^+	21^+	6527.8
635.7	0.6(3)	0.6		$E2$	20^+	18^+	5756.8
721.8	3.2(11)	3.2		$E2$	21^+	19^+	6131.0
771.0	1.7(7)	1.8		$E2$	22^+	20^+	6527.8
Decay of Band 2							
140.0					16^+		4725.7
150.1	0.6(3)	2.5		$M1$	17^+	16^+	4888.3
273.0	11(2)	17		$M1$	16^+	15^+	4725.7
581.7	2.7(10)	2.9		$M1$	21^+	20^+	6131.0
590.5	9.5(26)	10		$M1$	16^+	16^+	4725.7
614.8	6.3(19)	6.7		$M1$	19^+	18^+	5409.2
753.1	10(3)	11		$M1$	17^+	16^+	4888.3
797.0	0.6(3)	0.6		$(M1)$	(15^+)	14^+	4670.7
803.6							4585.7
1025.2	3.8(12)					14^+	4585.7
1080.2	3.8(13)	3.8		$(M1)$	(15^+)	14^+	4640.7
1165.2	3.2(12)	3.3		$E2$	16^+	14^+	4725.7
Band 3							
154.6	4.6(14)	17	$-0.25(10)$	$M1$			
223.3	2.1(8)	4.2		$(M1)$			
242.9	2.1(8)	3.7		$(M1)$			
285.8	2.3(9)	3.4		$(M1)$			
301.8	11(3)	16		$(M1)$			
387.7	7.0(18)	8.5	$-0.32(9)$	$M1$			
397.5	4.8(15)	5.8		$(M1)$			
401.4	10(3)	12		$(M1)$			
Band 4							
119.5	18(4)	119		$M1$	18^-	17^-	5105.2
145.0	29(6)	127		$M1$	19^-	18^-	5250.2
197.0	49(8)	118		$M1$	20^-	19^-	5447.2
260.2	57(8)	94		$M1$	21^-	20^-	5707.4
336.0	47(8)	63		$M1$	22^-	21^-	6043.4
367.0	1.0(5)	1.2		$(M1)$	(29^-)	(28^-)	8882.4
372.5	1.0(5)	1.2		$(M1)$	(30^-)	(29^-)	9254.9
376.0	30(6)	37		$M1$	23^-	22^-	6419.4
384.9	1.9(8)	2.3		$(M1)$	(28^-)	27^-	8515.4
416.8	18(4)	19		$M1$	24^-	23^-	6836.2
424.0	7.8(24)	9.2		$M1$	25^-	24^-	7260.2
428.5	3.0(12)	3.5		$M1$	27^-	26^-	8130.5
441.8	6.3(19)	7.3		$M1$	26^-	25^-	7702.0
596.2	6.1(20)	6.2		$E2$	22^-	20^-	6043.4
712.0	5.0(16)	5.1		$E2$	23^-	21^-	6419.4
792.8	3.9(14)	3.9		$E2$	24^-	22^-	6836.2
840.8	2.2(9)	2.3		$E2$	25^-	23^-	7260.2
865.8	2.3(9)	2.3		$E2$	26^-	24^-	7702.0
Decay of Band 4							
(24)[b]				$M1$	17^-	16^-	4985.7
294.0	3.5(10)	5.1		$M1$	17^-	16^-	4985.7
538.2	3.9(15)	4.0	0.3(2)	$E2$	17^-	15^-	4985.7

TABLE I. *(Continued.)*

$E_\gamma{}^{\text{a}}$ (keV)	I_γ	I_{tot}	a_2	Multipolarity	J_i^π	J_f^π	E_i (keV)
Band 4a							
256.2	2.9(10)	4.9		(M1)	21⁻	(20)⁻	6164.9
286.8	6.9(20)	10		(M1)	(22⁻)	21⁻	6451.7
335.4	9.0(32)	12		(M1)	23⁻	(22⁻)	6787.1
351.6	8.5(25)	11		(M1)	(24⁻)	23⁻	7138.7
362.0	6.0(20)	7.6		(M1)	(25⁻)	(24⁻)	7500.7
Decay of Band 4a							
457.5	2.4(10)	2.8		M1	21⁻	21⁻	6164.9
461.5	3.7(12)	4.3		M1	(20)⁻	20⁻	5908.7
743.7	5.9(15)	6.2	−0.34(9)	M1	23⁻	22⁻	6787.1
914.7	4.3(12)	4.3	0.4(1)	E2	21⁻	19⁻	6164.9
1004.5	1.3(7)	1.4		(E2)	(22⁻)	20⁻	6451.7
Decay to Band 4a							
230.0	1.2(6)						7412.1
395.0	2.8(11)					23⁻	7182.1
Band 5							
129.2	4.6(14)	26		M1	21⁻	20⁻	6122.2
196.3	11(3)	26		M1	22⁻	21⁻	6318.5
208.5	12(3)	27		M1	23⁻	22⁻	6527.0
270.0	14(4)	22		M1	24⁻	23⁻	6797.0
328.9	16(3)	21		M1	25⁻	24⁻	7125.9
363.0	13(4)	16		M1	26⁻	25⁻	7488.9
373.0	9.2(3)	11.5		M1	27⁻	26⁻	7861.9
387.9	2.9(12)	3.6		M1	29⁻	28⁻	8646.6
391.5	3.4(15)	4.1		(M1)	(30⁻)	29⁻	9038.1
396.8	8.4(24)	10		M1	28⁻	27⁻	8258.7
401.0	1.6(8)	1.9		(M1)	(31⁻)	(30⁻)	9439.1
Decay of Band 5							
192.4	2.4(10)				20⁻		5993.0
377.6	2.4(10)	3.0		M1	24⁻	23⁻	6797.0
483.6	1.2(5)	1.3		M1	23⁻	22⁻	6527.0
498.9	18(4)	20		M1	20⁻	19⁻	5993.0
753.6	3.9(10)	4.0	0.4(1)	E2	24⁻	22⁻	6797.0
Band 6							
143.2	7.5(19)	34		M1	15⁻	14⁻	4407.8
283.9	19(4)	29		M1	16⁻	15⁻	4691.7
361.0	14(3)	18		M1	17⁻	16⁻	5052.7
380.5	6.9(22)	8.5		M1	18⁻	17⁻	5433.2
384.8	3.3(12)	4.0		M1	19⁻	18⁻	5818.0
644.9	4.9(17)	5.0		E2	17⁻	15⁻	5052.7
741.5	3.0(10)	3.0		E2	18⁻	16⁻	5433.2
765.3	1.5(8)	1.5		E2	19⁻	17⁻	6198.5
Decay of Band 6							
(50)ᵇ					14⁻		4264.6
415.6	4.6(17)	5.5		M1	14⁻	13⁻	4264.6
537.9	23(4)	24		E2	14⁻	12⁻	4264.6
558.8	2.9(10)	3.0		E2	15⁻	13⁻	4407.8
Band 7							
202.1	1.6(7)	3.6		(M1)	(22⁻)	(21⁻)	6510.0
248.8	5.7(16)	10	−0.4(1)	M1	(23⁻)	(22⁻)	6758.8
276.0	4.7(13)	7.3		(M1)	(24⁻)	(23⁻)	7034.8
317.1	3.9(12)	5.4		(M1)	(25⁻)	(24⁻)	7351.9
363.2	3.0(10)	3.8		(M1)	(26⁻)	(25⁻)	7715.1

TABLE I. *(Continued.)*

E_γ [a] (keV)	I_γ	I_{tot}	a_2	Multipolarity	J_i^π	J_f^π	E_i (keV)
384.9	1.3(6)	1.6		$(M1)$	(27^-)	(26^-)	8100.0
413.0	0.6(3)	0.7		$(M1)$	(28^-)	(27^-)	8513
Decay of Band 7							
(84)[b]					(22^-)		6510.0
213.7	1.2(6)				(21^-)		6307.9
556.0	1.3(6)	1.4			(23^-)	21^-	6758.8
603.0	2.2(9)	2.4			(22^-)	21^-	6510.0
759.0	2.0(9)	2.1			(21^-)	20^-	6307.9
961.1	2.8(10)	2.8			(22^-)	20^-	6510.0
Group 1							
109.8	0.3(2)				21^+		6082.5
283.2	1.3(6)	2.0		$M1$	14^+	14^+	3843.7
291.5	1.7(7)	1.9		$E2$	16^+	14^+	4135.2
494.8	7.9(30)	8.1		$E2$	14^+	12^+	3843.7
516.9	6.7(21)				15^+		4452.7
553.7	3.3(11)						3935.8
567.6	5.4(14)				14^+		4503.4
574.7	177(20)	181		$E2$	16^+	14^+	4135.2
586.9	7.6(24)					12^+	3935.8
609.0	4.4(15)	4.7		$M1$	15^+	14^+	4452.7
644.0	2.1(9)						5972.7
646.0	2.6(10)						5328.7
659.2	100(11)	102		$E2$	18^+	16^+	4794.4
664.9	6.9(22)	6.9		$E1$	14^+	13^-	4503.4
668.4	1.6(7)	1.7		$M1$	14^+	14^+	4512.1
699.0	0.9(5)						6027.7
720.8	7.6(23)	7.9		$M1$	12^+	12^+	3348.9
754.0	4.4(20)					12^+	3382.1
754.9	36(6)	37		$E2$	20^+	18^+	5549.3
767.8	8.9(25)	9.0	0.2(1)	$E2$	12^+	10^+	3348.9
784.6	1.8(8)					22^+	7158.3
801.0	2.0(8)					10^+	3382.1
824.4	11(3)	11	0.16(10)	$E2$	22^+	20^+	6373.7
839.0	6.5(18)					14^+	4682.7
892.2	14(3)	14		$M1$	15^+	14^+	4452.7
932.4		400[c]		$E2$	14^+	12^+	3560.5
972.9	1.2(5)					22^+	7346.6
1042.2	1.3(6)					20^+	6591.5
1215.6		35[c]		$E2$	14^+	12^+	3843.7
Group 1a							
109.2	0.7(3)				21^+		5932.8
269.1	1.0(5)						6598.2
286.1	1.5(6)	2.3		$M1$	22^+	21^+	6218.9
296.9	0.8(4)					22^+	6560.3
341.4	2.3(9)					22^+	6560.3
379.3	1.2(6)					22^+	6598.2
396.3	1.7(6)					21^+	6329.1
452.5	0.5(3)					22^+	6715.9
461.6	41(6)	43	0.40(7)	$E2$	20^+	18^+	5256.0
497.0	2.1(7)					22^+	6715.9
544.8							6329.1
567.6	6.0(20)					20^+	5823.6
599.4							7035.4
676.8	6.4(20)	6.5	$-0.35(10)$	$M1$	21^+	20^+	5932.8
706.3	1.6(7)						7035.4
712.8	1.6(8)						7748.2

TABLE I. *(Continued.)*

$E_\gamma{}^{\text{a}}$ (keV)	I_γ	I_{tot}	a_2	Multipolarity	J_i^π	J_f^π	E_i (keV)
757.5	1.1(5)						7792.9
779.8	3.0(12)					20^+	6329.1
816.5	2.0(8)					22^+	7035.4
962.9	11(3)	11	0.16(9)	$E2$	22^+	20^+	6218.9
1007.4	6.2(17)	6.2	0.18(9)	$E2$	22^+	20^+	6263.4
1073.1	1.4(6)					20^+	6329.1
Group 2							
229.3	1.6(7)	3.0			16^+	16^+	4364.5
248.0	5.3(16)					16^+	4612.5
350.5							4612.5
354.0							4262.0
401.8							4262.0
402.7	7.2(23)					14^+	4612.5
406.4	3.0(11)				14^+		4209.8
461.0	7.4(25)	7.7	0.14(10)	$E2$	18^+	16^+	5199.2
479.9							4262.0
516.5	1.0(5)	1.0		$E2$	18^+	16^+	5199.2
520.8	4.7(16)	4.8	0.2(1)	$E2$	16^+	14^+	4364.5
528.4	4.0(14)	4.1	0.4(2)	$E2$	16^+	14^+	4738.2
562.6	3.1(11)	3.2		$E2$	14^+	12^+	4209.8
585.1							5784.3
586.7					18^+		5199.2
600.7$^{\text{d}}$	8.0(20)	8.2	0.3(1)	$E2$	14^+	12^+	4209.8
651.7							6436.0
768.8	2.6(9)					14^+	4612.5
804.0	4.4(20)	4.4	0.24(10)	$E2$	16^+	14^+	4364.5
894.5	3.3(12)	3.3			16^+	14^+	4738.2
1066.1	6.5(18)	6.5	0.18(9)	$E2$	12^+	10^+	3647.2
1154.0						12^+	3782.1
1222.3	4.3(14)					10^+	3803.4
1232.1						12^+	3860.2
1279.9						12^+	3908.0
Group 3							
(65)$^{\text{b}}$				$M1$	17^-	16^-	5112.8
(83)$^{\text{b}}$				$M1$	15^-	14^-	4447.5
110.6	2.4(12)				19^-		5494.1
150.6	5.4(14)	21.5	−0.22(8)	$M1$	17^-	16^-	5112.8
198.4	2.5(15)	5.9		$M1$	16^-	15^-	4962.2
205.0	1.8(8)					17^-	5383.5
216.3	0.8(4)	1.7		$M1$	17^-	16^-	5178.5
243.9	2.3(9)	4.1		$M1$	19^-	19^-	5494.1
254.9	4.4(15)	7.5		$M1$	16^-	15^-	4962.2
270.7	12(4)					17^-	5383.5
284.4	8.2(24)	12.5		$M1$	16^-	15^-	5048.2
315.6	4.4(14)	4.9	0.24(9)	$E2$	19^-	17^-	5494.1
342.8	6.3(15)	8.3		$M1$	15^-	14^-	4707.3
364.0	95(12)	120		$M1$	13^-	12^-	3838.5
399.3	7.3(19)	8.8	−0.35(7)	$M1$	15^-	14^-	4763.8
417.1	6.7(22)						5800.6
474.7	3.3(12)						6275.3
508.4	4.8(15)	4.9		$E2$	19^-	17^-	5494.1
514.7	168(16)	186		$M1$	16^-	15^-	4962.2
526.0	21(5)	23	−0.24(7)	$M1$	14^-	13^-	4364.5
542.0		140$^{\text{c}}$		$M1$	12^-	11^-	3474.5
597.7	3.7(11)	3.8		$E2$	16^-	14^-	4962.2
600.7	21(5)	22	−0.33(7)	$M1$	16^-	15^-	5048.2

TABLE I. *(Continued.)*

$E_\gamma{}^{a}$ (keV)	I_γ	I_{tot}	a_2	Multipolarity	J_i^π	J_f^π	E_i (keV)
609.0	202(21)	206		E2	15⁻	13⁻	4447.5
636.1	2.0(8)	2.0	0.3(1)	E2	17⁻	15⁻	5112.8
731.0	9.0(16)	9.0	0.34(7)	E2	17⁻	15⁻	5178.5
868.8	4.9(15)	5.0		E2	15⁻	13⁻	4707.3
890.0	8.3(18)	8.4		E2	14⁻	12⁻	4364.5
906.0		152[c]		E2	13⁻	11⁻	3838.5
925.3	7.9(25)	8.0	0.2(1)	E2	15⁻	13⁻	4763.8
Group 4							
326.2	89(10)	97		E2	18⁻	16⁻	4700.9
372.5	103(13)	129		M1	16⁻	15⁻	4374.7
375.9	7.8(20)	8.3		E2	19⁻	17⁻	5326.0
459.7	11(3)	11		E2	20⁻	18⁻	5548.9
473.9	3.7(13)	3.8		E2	18⁻	16⁻	5089.2
486.3	3.9(9)					19⁻	5812.3
575.4	4.2(15)	4.5		M1	17⁻	16⁻	4950.1
581.0	13(3)	13.5	0.24(10)	E2	21⁻	19⁻	5907.0
596.6	43(6)	44		E2	17⁻	15⁻	4598.8
613.1	18(3)	19		M1	16⁻	15⁻	4615.3
653.9	17.5(3.3)	18.5	−0.32(7)	M1	21⁻	20⁻	6202.8
665.4	2.1(8)					20⁻	6572.4
666.8	1.7(7)					20⁻	6426.5
697.1	2.1(8)					20⁻	6426.5
699.0	2.8(9)					20⁻	6641.2
714.5	14(3)	14	0.32(10)	E2	18⁻	16⁻	5089.2
727.2	18(4)	19	0.26(7)	E2	19⁻	17⁻	5326.0
758.4	7.8(23)					20⁻	6961.2
760.0	6.0(17)					20⁻	6489.4
760.1	2.5(7)						6572.4
768.2	2.8(10)					19⁻	6094.2
772.1	1.8(8)						7413.3
791.8	1.9(8)						7433.0
814.0	2.3(9)						7775.2
818.0	4.5(15)						7307.4
818.1	2.0(8)						7390.4
848.0	27(5)	27	0.25(7)	E2	20⁻	18⁻	5548.9
861.0	2.2(9)						7822.2
866.7	2.2(9)						8174.1
911.8	1.5(7)					20⁻	6641.2
947.9	7.0(20)	7.1	0.16(9)	E2	17⁻	15⁻	4950.1
1028.5	17(4)	17	0.22(7)	E2	20⁻	18⁻	5729.4
1058.8	2.7(10)	2.7	0.2(1)	E2	20⁻	18⁻	5759.7
1056.7	7.3(23)					15⁻	5058.9
1123.3	2.6(10)					18⁻	5824.2
1241.3	4.0(14)	4.0	0.4(1)	E2	20⁻	18⁻	5942.2
Decay to 12⁺							
158.5	8.9(25)	10		E1	15⁻	14⁺	4002.2
441.7	198(26)	200		E1	15⁻	14⁺	4002.2
Group 5							
178.3	13(3)	38		M1	8⁻	7⁻	2419.5
215.0	1.4(6)	3.0	−0.3(2)	M1	16⁻	15⁻	4691.7
260.5	15(3)	24		M1	8⁻	7⁻	2501.7
323.0	0.7(4)						5375.7
357.9	5.4(20)	5.8		E2	11⁻	9⁻	3271.2
365.5	16(4)					13⁻	4214.5
415.8	2.5(10)	3.0		M1	16⁻	16⁻	5107.5
455.5	4.4(14)	5.0		M1	12⁻	11⁻	3726.7

TABLE I. *(Continued.)*

$E_\gamma{}^{\text{a}}$ (keV)	I_γ	I_{tot}	a_2	Multipolarity	J_i^π	J_f^π	E_i (keV)
459.5	8.7(25)	9.0		$E2$	11^-	9^-	3372.8
476.2	3.3(1)	3.4		$E2$	13^-	11^-	3849.0
519.7	39(4)	40		$E2$	12^-	10^-	3726.7
564.5	5.5(2)					16^-	5672.0
577.8	38(5)	39		$E2$	13^-	11^-	3849.0
627.7	13(3)	13		$E2$	15^-	13^-	4476.7
630.8	5.1(18)	5.2	0.4(1)	$E2$	17^-	15^-	5107.5
672.1	17(3)	17		$E2$	9^-	7^-	2913.3
705.3	12(3)	12		$E2$	10^-	8^-	3207.0
787.5	23(4)	24		$E2$	10^-	8^-	3207.0
799.5	10(3)	11		$M1$	10^-	9^-	3207.0
863.7	46(6)	47	0.26(7)	$E2$	11^-	9^-	3271.2
Group 6							
(43)$^{\text{b}}$					13^+		4375.1
(59)$^{\text{b}}$					13^+		4375.1
139.7				$M1$	13^+	12^+	4375.1
171.8	0.5(3)						4332.2
352.0	6.4(20)	8.2		$M1$	10^+	9^+	3282.4
465.0	5.1(15)	5.8		$M1$	12^+	11^+	4235.4
488.0	5.5(16)	6.1		$M1$	11^+	10^+	3770.4
493.2	18(4)	20		$M1$	9^+	8^+	2930.4
505.5	0.8(4)						4315.8
521.9	0.9(5)						4332.2
533.7$^{\text{e}}$							4315.8
536.6	25(4)	25		$E1$	13^+	13^-	4375.1
550.1$^{\text{e}}$							4332.2
614.4							3544.8
615.6							4160.4
664.0	15(3)					6^+	2799.1
668.6$^{\text{f}}$	1.5(6)					12^+	4315.8
671.3	5.3(17)						3470.4
685.0$^{\text{f}}$	1.8(8)					12^+	4332.2
706.7	4.5(14)					12^+	4315.8
722.5	3.2(11)						3521.6
723.1	5.0(16)					12^+	4332.2
751.7	0.6(3)						4315.8
765.0	2.2(8)						3564.1
768.1	0.9(4)						4332.2
794.2	0.9(4)						4315.8
810.6	1.4(6)						4332.2
840.0	6.8(20)	6.9		$E2$	11^+	9^+	3770.4
845.2	14(3)	14		$E2$	10^+	8^+	3282.4
845.4	2.2(8)						4315.8
857.7	13(3)					12^-	4332.2
861.8	1.6(7)						4332.2
953.0	6.1(17)	6.1		$E2$	12^+	10^+	4235.4
981.0				$M1$	12^+	12^+	3609.1
1028.0	8.5(20)	8.5	0.38(9)	$E2$	12^+	10^+	3609.1
1229.2	2.3(9)					10^+	3810.3
1302.9				$E1$	12^+	11^-	4235.4
1399.7						11^-	4332.2
1687.7						12^+	4315.8
1704.1						12^+	4332.2
Yrast							
(47)$^{\text{b}}$				$E2$	12^+	10^+	2628.1
106.1	2.4(10)	3.4		$E1$	7^-	6^+	2241.2
166.3	49(7)	91		$E2$	9	7^-	2407.5

TABLE I. *(Continued.)*

E_γ[a] (keV)	I_γ	I_{tot}	a_2	Multipolarity	J_i^π	J_f^π	E_i (keV)
173.6	30(4)	33		$E1$	10^+	9^-	2581.1
196.0	10(3)	11		$E1$	8^+	7^-	2437.2
280.1	201(20)	208		$E1$	5^-	4^+	1820.3
302.1	25(4)	28		$E2$	8^+	6^+	2437.2
304.4				$E1$	11^-	12^+	2932.5
351.4				$E1$	11^-	10^+	2932.5
420.9	186(17)	194		$E2$	7^-	5^-	2241.2
495.3				E3	11^-	8^+	2932.5
575.1	257(28)	263		$E2$	4^+	2^+	1540.2
594.9	48(8)	49		$E2$	6^+	4^+	2135.1
965.1		270[c]		$E2$	2^+	0^+	965.1

[a]Uncertainties between 0.3 and 1.0 keV depending on intensity.

[b]Transition deduced from the coincidence relationships.

[c]Value used for intensity normalization (see text).

[d]Transition not shown in the level scheme. The final level is in group 6 at 3609.1 keV.

[e]Transition not shown in the level scheme. The final level is in group 2 at 3782.1 keV.

[f]Transition not shown in the level scheme. The final level is in group 2 at 3647.2 keV.

a rearrangement in the low-spin part (at the bandhead). The 819.6-keV transition placed in Ref. [19] above the 754.9-keV transition parallel to the 260.7-keV transition is in fact in coincidences with the 260.7-keV transition and the transitions above it. This fixes levels at 6368.9 and 6629.6 keV as members of band 1. The 255.9-keV transition links the 6629.6-keV level to the 6373.7-keV level of the strongest sequence of group 1. Furthermore, the 6368.9-keV level depopulates via a new 286.4-keV transition into the 6082.5-keV level of a new branch of group 1. The positive value of the a_2 angular distribution coefficient of the 819.6-keV transition allows for an $E2$ multipolarity leading to spin-parity 22^+ for the 6368.9-keV level. With these connections the energies of all levels of band 1 are changed with respect to Ref. [19] and a gap of 124.1 keV emerges above the 4642.3-keV level. Since no transition of 124 keV was observed in coincidences with the transitions of band 1 and/or the low-spin levels, we suppose an existence of a level between the 4766.4- and 4642.3-keV levels. Possible candidates for two low-energy transitions were found in our 1-MeV cube. Transitions with energies of 58.3 and 65.5 keV were clearly seen in coincidences with only the transitions of band 1. An estimate of their intensities in the double gate 130.2–137.0 keV allows for a placement of these transitions at the bottom of band 1 (in the gap) provided the multipolarity of both is $M1$. As can be seen from Fig. 2 (Parts A and C) the 58.3-keV transition may contain an intensity from the (59)-keV transition of group 6. The contribution of the latter has been estimated from the depopulation balance of the 4642.3-keV level to be less than 11% of the intensity of the 58.3-keV transition. Searching for transitions depopulating the level in the gap we found one uncontaminated of 248.3 keV to the 15^+ level at 4452.7 keV of group 1. Thus a level at 4700.9 keV was established, defining the correct order of 65.5- and 58.3-keV transitions (see Table I). The tentative (64)-keV transition placed in Ref. [19] in their group B in fact does not exist,

as will be discussed later (see also group 2 in Fig. 2, Part B).

Two summed γ-ray coincidence spectra are shown in Figs. 3(a) and 3(b). These illustrate the new features of band 1, in particular its depopulation from low- and high-spin states. With the described changes the bandhead of band 1 cannot be the 13^+ level at 4375.1 keV as accepted in Ref. [19]. The 15^+ level at 4642.3 keV is a reasonable candidate for a bandhead of band 1. Above the 17^+ level, band 1 in ^{194}Pb looks very similar to band 1 in ^{196}Pb [18] (up to spin 29^+). The depopulation of band 1 in ^{196}Pb below a spin 17^+ is rather complex so this band is discussed above this spin in Ref. [18].

Some changes in the band called 2c in Ref. [19] feeding into the low-spin part of band 1 had to be made, resulting in two branches of low-energy transitions (bands 1a and 1b in Fig. 2, Part A). They are interconnected via the 304.7-keV transition and a new 383.8-keV transition and feed into band 1 at spins 20^+, 21^+. We observed two new high-energy transitions of 785.6 and 793.1 keV depopulating bands 1a and 1b, respectively. The tentative crossover transitions of 699 and 757 keV suggested in Ref. [19] were not observed.

The depopulation of band 1 below the 15^+ level proceeds mainly through the 4375.1-keV level in a rather fragmented way: to the levels of the 11^- isomer (35%), to the levels of groups 2 and 6 feeding the 10^+ and 12^+ isomers (31%), to the levels of group 6 built on the 8^+ yrast state (21%), and to a weak new branch of group 6 by-passing the 10^+ and 12^+ isomers down to the 6^+ yrast state (3%). The population of the levels of group 1 is about 9%. In group 6 we added a level at 4315.8 keV that is connected with the 4375.1-keV level by an unobserved (59)-keV transition. The new level allows for a correct placement of the 1687.7- and 1154.0-keV transitions, which now feed the 12^+ isomer and excludes the existence of a (64)-keV transition placed in Ref. [19]. The order of 533.7- and 1154.0-keV transitions is reversed and confirmed
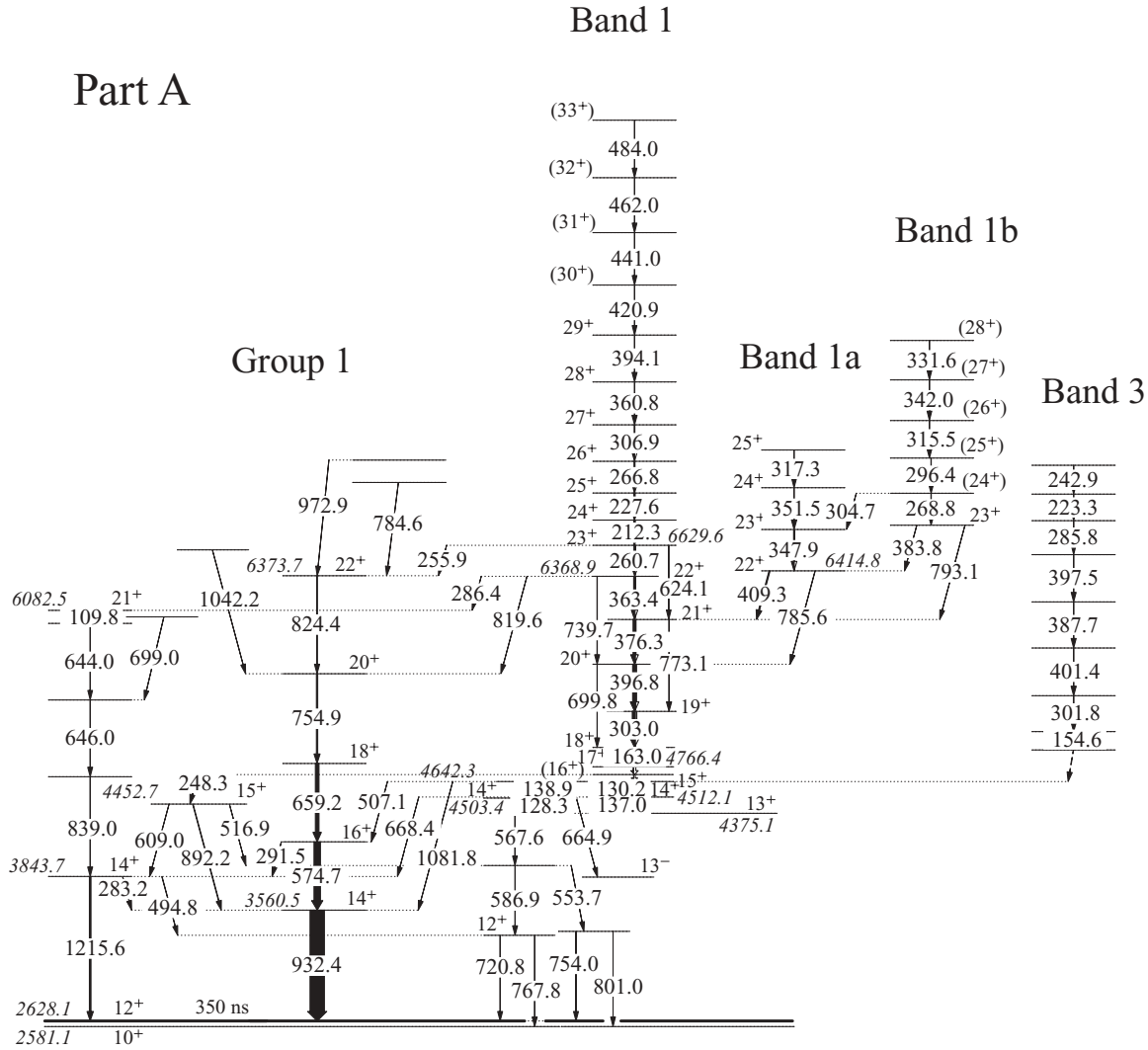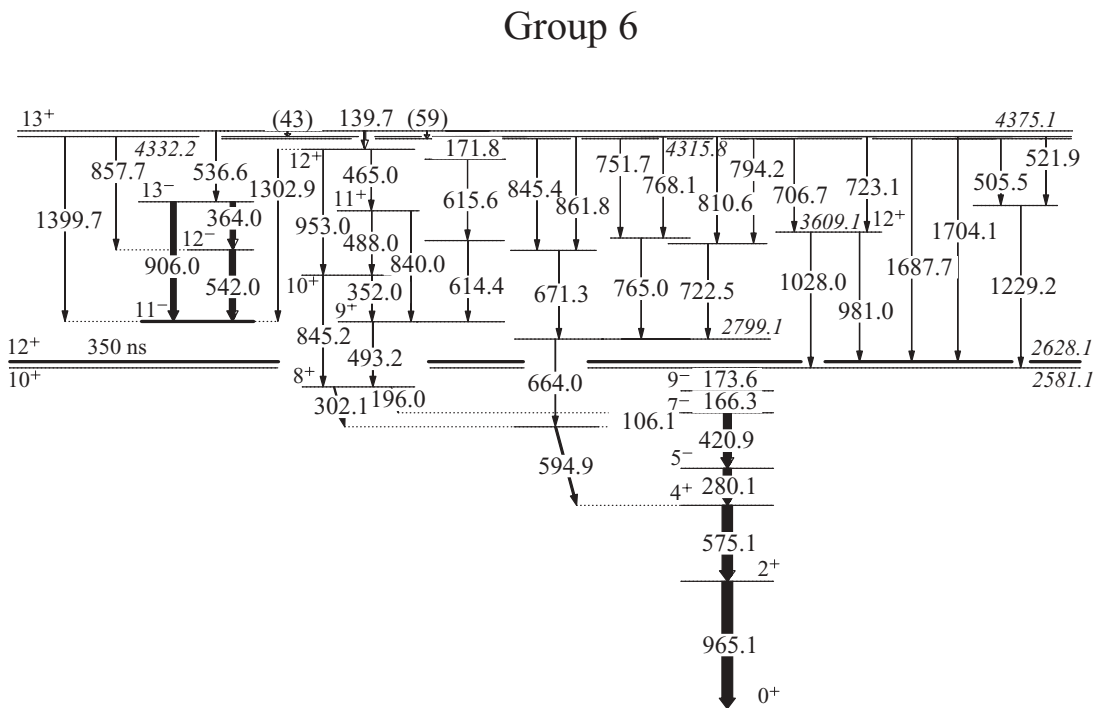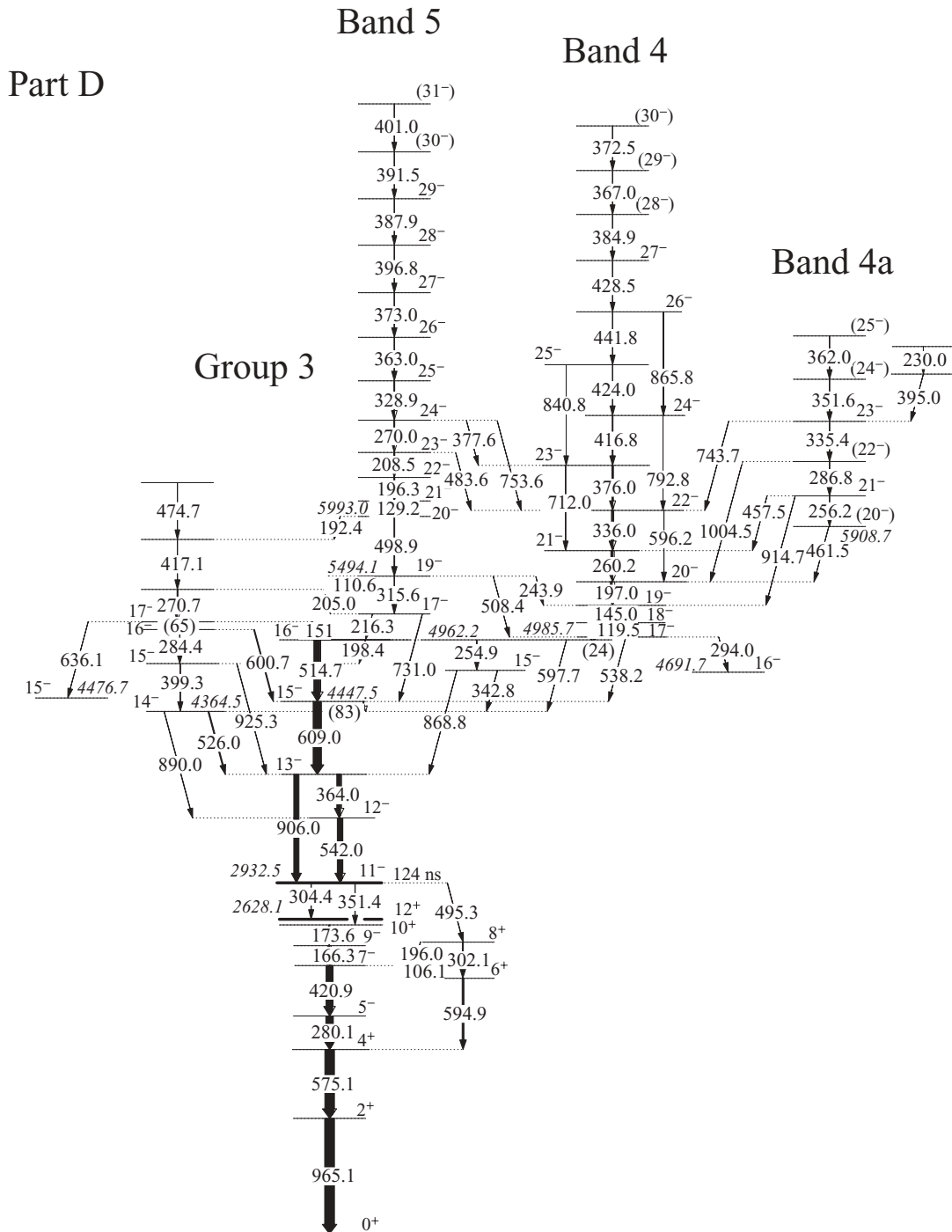
FIG. 1. The positive-parity part of the level scheme of ^{194}Pb deduced from the present experiment (Parts A–C). The energies are given in keV. A fragment of levels built on the 11$^-$ isomer is exposed within group 6 (Part C) and group 1 (Part A) to show their population from the positive-parity levels.

by several new connections from groups 2 and 6 and band 2 (see Fig. 2, Parts B and C, and Table I). It should be noted that the division into groups in the positive-parity part of the level scheme is rather conditional as they are interconnected by many transitions.

2. Band 3

Observed is a new weak sequence of transitions, band 3, that de-excites in a very similar way as band 1 below the 15$^+$ level at 4642.3 keV, as shown in Fig. 3(c). It is, however not clear, whether the 154.6-keV transition should be placed directly on top of this level. As the first few transitions of band 3 are very close in energy to those of band 1 we expect that the level populated by the 154.6-keV transition belongs to band 3 and that there is an additional transition(s) depopulating this band down to the 4642.3-keV level. This band is the only one that could not be connected exactly to the lower lying levels.

3. Band 2

Band 2 has been established in Ref. [19] (denoted band 3). Several new transitions have been added to band 2 and to its decay scheme in the present work (see Fig. 2, Part B). A 371.5-keV transition was resolved in the complex peak at 375 keV by using appropriate coincidences and placed above the 377.2-keV transition. The new depopulating transitions of 1080.2 and 797.0 keV observed in coincidences with the transitions of band 2 feed into the 14$^+$ levels of group 1 at 3560.5 and 3843.7 keV, respectively, defining a new level at 4640.7 keV. We suggest this level to be the (15$^+$) level of band 2. The (85)-keV transition between the 16$^+$ and the new (15$^+$) level cannot be resolved in the X-ray background. Band 2 decays predominantly to the spherical states of group 1. Additional new linking transitions are of 581.7, 516.9, 609.0, and 1025.2 keV. We found also links from the low-spin part of band 2 to the levels of the new structure, group 2 (150.1 and 140.0–803.6 keV). A spectrum of band 2 is shown in Fig. 4.

Part B

Band 2

Group 1a

Group 2

(25^+) 361.0
(24^+) 371.5
(23^+) 377.2
22^+

712.8 757.5
599.4 706.3 816.5
269.1 379.3 341.4 497.0 296.9 452.5 22^+
651.7 544.8 396.3 22^+ 286.1 771.0 396.8 21^+
779.8 109.2 21^+ 374.2 721.8 581.7 6082.5 21^+ 109.8
585.1 1073.1 962.9 676.8 567.6 1007.4 635.7 347.6 19^+ 644.0 5549.3 20^+
461.0 16^+ 586.7 516.5 20^+ 461.6 5256.0 288.1 614.8 646.0 754.9
4738.2 18^+ 150.1 16^+ 162.6 753.1 18^+
4612.5 350.5 402.7 528.4 16^+ 16^+ 140.0 232.8 17^+ 659.2 18^+
4262.0 354.0 479.9 406.4 14^+ 4209.8 248.0 4364.5 894.5 803.6 4452.7 273.0 (85.0) 16^+ 797.0 590.5 839.0 16^+
401.8 562.6 12^+ 520.8 229.3 768.8 1025.2 609.0 15^+ (15^+) 4640.7 1080.2 1165.2 291.5 574.7
1279.9 3782.1 804.0 3647.2 892.2 15^+ 14^+ 283.2 14^+
1232.1 1154.0 1222.3 1066.1 12^+ 12^+ 3843.7 3560.5
12^+ 350 ns 1215.6 932.4
10^+ 2628.1 2581.1

FIG. 1. *(Continued.)*

Part C

Group 6

13^+ (43) 139.7 (59) 171.8 751.7 4315.8 794.2 4375.1
4332.2 857.7 536.6 12^+ 465.0 615.6 845.4 768.1 706.7 723.1 521.9
1399.7 13^- 364.0 1302.9 11^+ 953.0 861.8 810.6 3609.1 505.5
12^- 906.0 542.0 488.0 840.0 765.0 722.5 1028.0 12^+ 1704.1 1687.7 1229.2
11^- 10^+ 352.0 614.4 671.3 2799.1 981.0 2628.1
12^+ 350 ns 845.2 9^+ 2581.1
10^+ 493.2 664.0 9^- 173.6
8^+ 302.1 196.0 7^- 166.3 106.1
594.9 420.9
5^- 280.1
4^+ 575.1
2^+ 965.1
0^+

FIG. 1. *(Continued.)*

FIG. 2. The negative-parity part of the level scheme of ^{194}Pb deduced from the present experiment (Parts D and E). The energies are given in keV. The levels at 4691.7 keV of band 6 and 4476.7 keV of group 5 are displayed also in Part D to include connections between the two parts.

B. Negative-parity bands

1. Band 5

In the negative-parity part of the level scheme, presented in Fig. 2 (Parts D and E), the major changes concern band 5. It contains the two fragments called band 1b and band 1c in Ref. [19]; these are now arranged in one sequence. Analyzing the three-dimensional data (cubes) allowed us to find many connections to previously known or newly observed low-lying levels of group 3 (group A in Ref. [19]), so that the bandhead of this band had to be shifted by more than 0.5 MeV upward. We added two new transitions on top of band 5. The new levels placed below the bandhead allow for a correct bandhead energy and spin. Since the multiplicity of the new 315.6- and 731.0-keV transitions is compatible with stretched *E*2 the parity of the band is negative, as in Ref. [19]. Now band 5
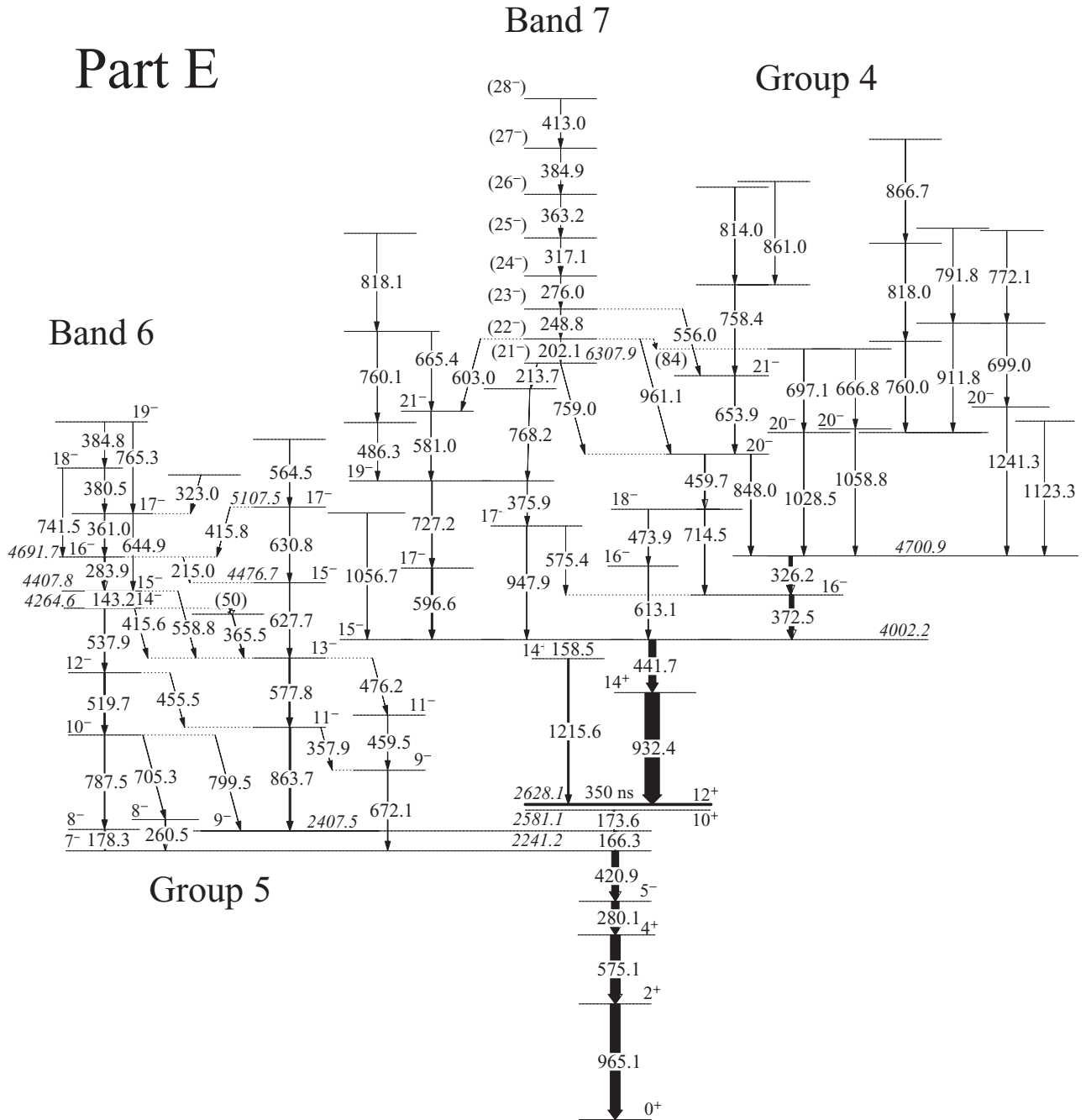
FIG. 2. *(Continued.)*

becomes the analog to band 3 of ^{196}Pb. Also the decay from the levels of band 5 into band 4 suspected in Ref. [19] could be established. A population into the lowest levels of band 4 from the 5494.1-keV level of group 3 is also observed. Spectra gated in a way to show these described connections between bands 4 and 5 and group 3 are shown in Fig. 5.

2. Band 4

The observed linking transitions from band 5 require in turn that the lowest level of band 4 (denoted band 1a in

Ref. [19]) to be shifted by 24 keV above the 4962.2-keV level compared to that in Ref. [19]. The resulting 4985.7-keV level is further confirmed by the 538.2-keV transition to the 15$^-$ (4447.5-keV) level of group 3 and by the 294.0-keV transition to the 16$^-$ (4691.7-keV) level of band 6. The spin assignment of 17$^-$ for the bandhead of band 4 at 4985.7 keV results from its connections with the 19$^-$ level at 5494.1 keV (508.4-keV transition) and the 15$^-$ level at 4447.5 keV (538.2-keV transition). Band 4 is extended by the 367.0- and the 372.5-keV transitions to spin 30$^-$ and by the two crossover transitions of 596.2 and 865.8 keV. It depopulates predominantly to the levels of group 3 via the
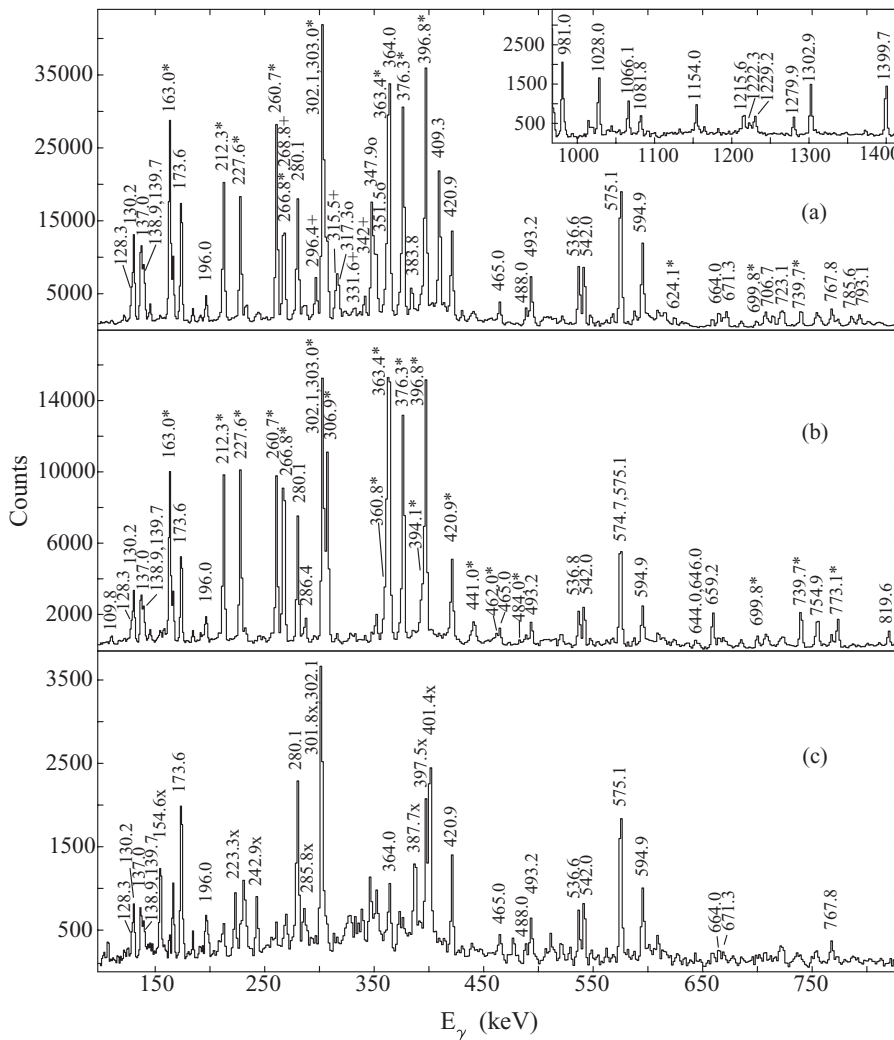
FIG. 3. Summed double-gated γ-ray coincidence spectra of (a, b) band 1 and (c) band 3. (a) Sum of the double-gated spectra on all transitions of band 1 [marked by asterisks (*)] below spin 22^+ to emphasize the connections to band 1a [marked by circles (o)] and band 1b [marked by plus signs (+)]. The strongest transitions of groups 1, 2, and 6 are also indicated in the spectrum and in the inset. (b) The summed coincidence spectrum of band 1 above spin 22^+ displays the high-spin part of band 1 and its depopulation from the 22^+ level to the states of group 1. (c) Spectrum of band 3 (marked by x symbols). Gates were set on all combinations of double gates, except 397.5–301.8 and 397.5–387.7 keV to avoid contamination from the strong bands 1 and 5, respectively. Some transitions of the groups 1, 2, and 6 are also shown to illustrate the similarity in the decay of bands 1 and 3.

unobserved (24)-keV transition. Group 3 is also extended by a new sequence built on the known 14^- level at 4364.5 keV. A sequence of four new low-energy transitions is arranged in a new band 4a, which has several connections to band 4.

3. Bands 6 and 7

Four low-energy transitions (143, 284, 361, and 380 keV) have been observed in Ref. [19], and the corresponding levels

were assigned to an irregular group (group 5 in the present work). We found a new transition of 384.8 keV in coincidences with these transitions and three crossover transitions of 644.9, 741.5, and 765.3 keV, which suggests a dipole band built on the 14^- level at an energy of 4264.6 keV. Band 6 and its depopulation to states of group 5 is very similar to the low-spin part of band 6 in ^{196}Pb. We also added a few new levels and transitions to group 5. From the angular distributions of the 215.0- and 630.8-keV transitions we deduced spins of 15^- and
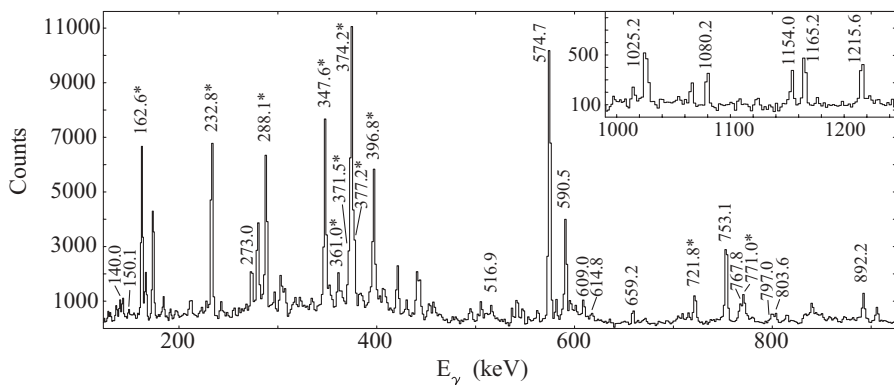
FIG. 4. Summed γ-ray coincidence spectrum of band 2. Double gates were set on all transitions up to a spin of 21^+. The transitions within the band 2 are marked by asterisks (*). The transitions depopulating band 2 are also shown in the spectrum and in the inset for the high-energy part.
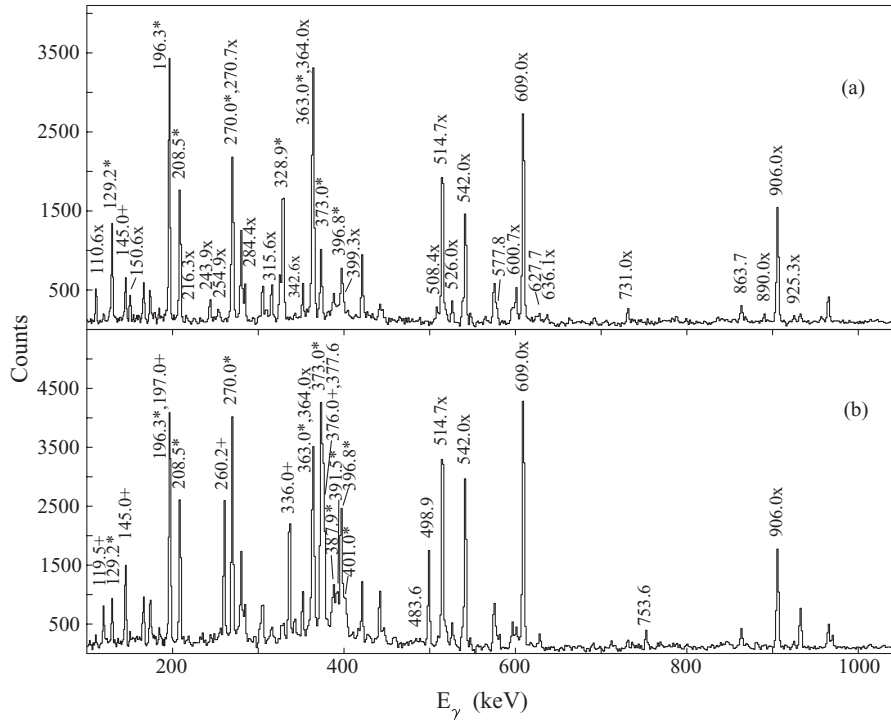
FIG. 5. Summed γ-ray coincidence spectra related to bands 4 and 5 and group 3. (a) Spectrum obtained by setting gates on the 498.8-keV transition and the 208.5- and 270.0-keV transitions of band 5 [marked by asterisks (*)] to show the low-spin connections with group 3 (marked by x symbols). (b) Spectrum obtained by setting double gates on all transitions of band 5 above the 24$^-$ level to emphasize the links between bands 5 and 4 [marked by plus signs (+)].

17$^-$ for the 4476.7- and 5107.5-keV levels, respectively, which confirms the tentative assignments proposed in Ref. [23]. The newly observed connecting transition of 476.2 keV leads to spin-parity assignment of 11$^-$ for the 3372.8-keV state.

Band 7 was observed as band 4 in Ref. [19], but was not linked to the normal states. We found many weak transitions connecting this band to the levels of group 4 and determined the excitation energy of the bandhead at 6307.9 keV. As will

be discussed later bands 6 and 7 may form a single band below and above the band crossing. Since band 7 is very weak and decays close to the bandhead it was not possible to detect the (two) transitions connecting band 7 to band 6. With these data, a tentative spin-parity assignment of (21$^-$) to the bandhead of band 7 at 6307.9 keV is suggested. Spectra of bands 6 and 7 are shown in Fig. 6. Group 4 is also extended to higher energies and spin assignments are made for several levels.
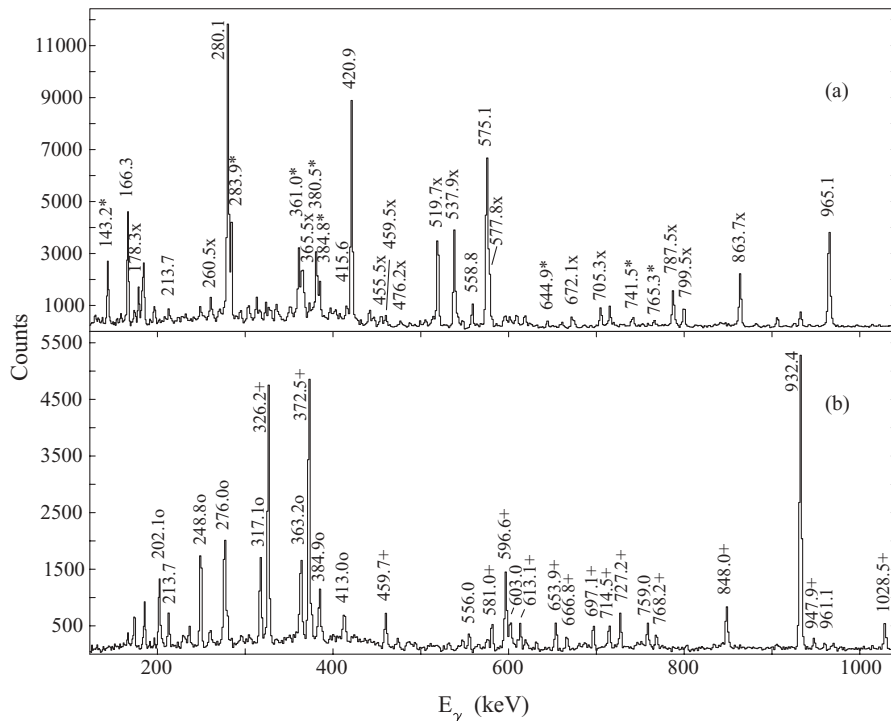
FIG. 6. Summed γ-ray coincidence spectra of bands 6 and 7. (a) Spectrum gated on all transitions of band 6 [marked by asterisks (*)]. Transitions belonging to group 5 are marked by x symbols. (b) Spectrum gated on the 441.7-keV transition and one of the transitions of band 7 [marked by circles (o)]. The transitions of group 4 are marked by plus signs (+).

IV. DISCUSSION

A. Low-lying states

The nucleus ^{194}Pb lies in the vicinity of the doubly magic ^{208}Pb, having a closed $1h_{11/2}$ proton shell at $Z = 82$ and a closed $3p_{1/2}$ neutron subshell. Thus, a spherical shape at its ground state and the low-lying yrast states being of mainly neutron two-quasiparticle (2qp) configurations is expected. Some quadrupole vibrational collectivity for the first 2_1^+ and 4_1^+ in such semi-magic nuclei is also a usual behavior. Indeed, the quasiparticle multistep shell-model calculations [25,26] reproduce by almost pure neutron 2qp configurations the $5_1^-[\nu(i_{13/2}^{-1}p_{3/2}^{-1})]$, $7_1^-[\nu(i_{13/2}^{-1}p_{3/2}^{-1})]$, $9_1^-[\nu(i_{13/2}^{-1}f_{5/2}^{-1})]$, $10_1^+[\nu(i_{13/2}^{-2})]$, and $12_1^+[\nu(i_{13/2}^{-2})]$ states. The first 2^+ and 4^+ states are not pure 2qp states but are described as "collective" ones [25,26], as may be expected. It is further assumed that they are mixed with intruder proton excitations, which is known to force the nucleus to a stable oblate deformation [26]. Such a mixing is proposed for the 2_1^+, 4_1^+, and 6_1^+ states in Ref. [27], because the unperturbed energies of the spherical neutron 2qp states and the deformed proton 2qp states are very close to each other. The intruder proton configuration of $(s_{1/2}^{-2}h_{9/2}^2)$ is proposed to be the main configuration for the 0_2^+ state [27–29] (at 931 keV; not seen in the present experiment) and for the 8_1^+ state (e.g., Ref. [8] and references therein), and g-factor measurements [5] revealed a $\pi(s_{1/2}^{-2}h_{9/2}^1i_{13/2}^1)$ configuration for the 11_1^- isomer. As previously mentioned, excitations across the $Z = 82$ gap to these intruder proton orbitals are known to drive the nucleus to stable collective oblate shapes. So, one may expect rotational bands on top of these states. However, such bands have not been observed. In the present experiment a very rich and complicated level structure in the irregular parts (groups) of the level scheme is established. The levels calculated as pure four-quasineutron excitations in Ref. [25] are compared with the experimental levels of ^{194}Pb in Ref. [19]. In view of some changes in the present level scheme, we should remark that (i) the level at 3348.9 keV of group 1 assumed to be the 11^+ state is now assigned spin 12^+, (ii) the yrast 20^+ state is according to the present study the 5256.0-keV level of group 1a, and not the 5549.3-keV state of group 1, (iii) the 14^- state at 4264.6 keV is the bandhead of the dipole band 6 (with a possible candidate for a spherical 14^- state being the new 4214.5-keV level of group 5), and (iv) the yrast 20^- state is now the 5548.9-keV level of group 4. It is argued in Ref. [25] that the agreement with the experimental level energies is improved when experimental energies of the first 2^+, 4^+, and 6^+ states are used in the calculations; this supports the idea of admixtures to the high-spin states from proton core excitations [26]. Obviously, detailed calculations with the inclusion of proton excitations across the gap are necessary to describe the irregular part of the level scheme. We expect that the present data will stimulate theoretical analyses of the complicated level system of the nucleus ^{194}Pb.

B. Magnetic bands

Together with the multiplet-like four-quasiparticle structures, bandlike regular sequences of very intense $M1$ transitions with weak or even nondetectable $E2$ transitions were observed. Such sequences were found for the first time in ^{199,200}Pb by Baldsiefen *et al.* [8] and were called "shears bands" or magnetic rotational (MR) bands. They are built on weakly deformed oblate states and manifest a completely new way of generating the nuclear spin. In the Pb isotopes MR bands occur when high-spin proton particles are coupled to high-spin neutron holes. Along the bands angular momentum is generated by a step-by-step alignment of the proton and neutron spins in the direction of the total angular momentum. As a result of the shears mechanism the $B(M1)$ values decrease with increasing spin [10]. In Ref. [8] the multiplet-like structures and the collective rotational bands were called "normal" to distinguish between them and the MR bands. Particularly in the Pb region, the MR bands result from a coupling of $h_{9/2}$ and $i_{13/2}$ proton particles to $i_{13/2}$ neutron holes. We exploit the nomenclature introduced in Ref. [8] as well as the results from the TAC calculations reported in Ref. [18] for band-configuration assignments. Since for the neutrons the pairing is taken into account in the TAC calculations, the standard cranked shell-model notations are used. The neutron configurations are labeled by the letters A, B, C, and D for the quasineutrons of $i_{13/2}$ origin, and E, F, . . . for the natural-parity quasineutrons (mainly $p_{3/2}$ and $f_{5/2}$). As there are only a few protons involved above the $Z = 82$ gap, the proton pairing is neglected. Thus, the proton configuration is only given by its spin quantum number. For example, a coupling of $\nu i_{13/2}^{-2}$ to $\pi(h_{9/2}^2)8^+$ excitation would be labeled AB8.

1. Positive-parity dipole bands

Configuration assignments have been made in a previous work [19] to the positive-parity bands in ^{194}Pb. Band 1 (denoted bands 2a and 2b in Ref. [19]) has been assigned configuration AE11 below and ABCE11 above the band crossing. The same configurations have been given to band 1 in ^{196}Pb [18] and band 1 in ^{198}Pb [30]. These bands show a band crossing at $\hbar\omega \sim$ 0.3 MeV and an alignment gain of $\sim$8$\hbar$, which is characteristic for an alignment of a BC pair. In Fig. 7, the spin as a function of rotational frequency for the positive-parity bands in ^{194}Pb is plotted together with the positive-parity bands in ^{196}Pb. With the modifications made to the excitation energy and spin of band 1, which previously would lie higher in excitation than band 1 in ^{196}Pb, the similarity of alignment behavior of bands 1 in both nuclei is more pronounced than before. Thus, we also concur with the AE11 assignment for band 1, which is crossed by the ABCE11 configuration. The new band 3 in ^{194}Pb decays apparently into the bandhead of band 1 (see Fig. 3). There is a striking similarity between the first few level spacings of band 3 and band 1 above spin 17^+ of the latter. Band 3 is very weak and lies probably at higher excitation energy than band 1. It may decay by more than one transition down to the bandhead of band 1. The most probable spin and parity of the first observed level of band 3 is 16^+ or 17^+. We included band 3 in Fig. 7 by assuming spin 17^+. It can be seen that the alignment behavior of bands 1 and 3 is very similar. From the decay and the alignment pattern a configuration involving the next available natural-parity neutron excitation AF11 can
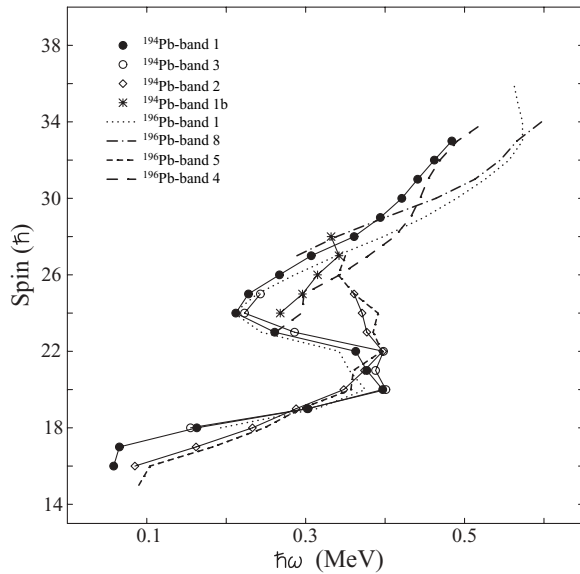
FIG. 7. Angular momentum vs rotational frequency of positive-parity bands in ^{194}Pb.

FIG. 8. Angular momentum vs rotational frequency of negative-parity bands in ^{194}Pb.

be suggested for band 3. The band crossing occurs at the same frequency as in band 1 and the onset of the ABCF11 configuration for band 3 is observed. In Fig. 7 band 8 of ^{196}Pb, which has been assigned ABCF11 configuration [18], is presented. This band could not be established before the crossing. However, in ^{198}Pb band 5 has been identified as AF11 below and ABCF11 configuration above the crossing [30].

The short new band 1b decays directly and via the structure 1a to band 1 below the band crossing. It has smaller alignment than bands 1 and 3. TAC calculations performed for ^{196}Pb in Ref. [18] predict that, at higher spin (around the first band crossings), the configuration ABCG11 is almost as favorable as ABCD8, ABCE11, and ABCF11. Consequently, an ABCG11 configuration may be assigned to the next observed band in this spin-energy region. The same configuration is given to band 4 of ^{196}Pb (see Fig. 7). Band 1 starts to upbend at $\hbar\omega =$ 0.45 MeV and gains an angular momentum of about $3\hbar$. This alignment reaches the one of band 4 in ^{196}Pb (see Fig. 7) in the frequency region where the latter is assigned an ABCEFG11 configuration [18]. Thus, it may be suggested that band 1 is crossed at high spins by the ABCGEF11 band. Band 2 was extended by two transitions with respect to Ref. [19] (named band 3 in that paper) but the excitation energy and spin are unchanged. Therefore we adopt the configurations of AB8 and ABCD8 before and above the band crossing given in Ref. [19]. Band 2 is an analog of band 5 in ^{196}Pb [18], where the same configuration AB8/ABCD8 was proposed. The alignment in these bands is not completed in both nuclei but it starts at higher frequency expected for a CD pair (see Fig. 7).

2. *Negative-parity dipole bands*

The spins as a function of rotational frequency for the negative-parity bands in ^{194}Pb are plotted in Fig. 8 and compared with similar bands in ^{196}Pb. The configuration AB11
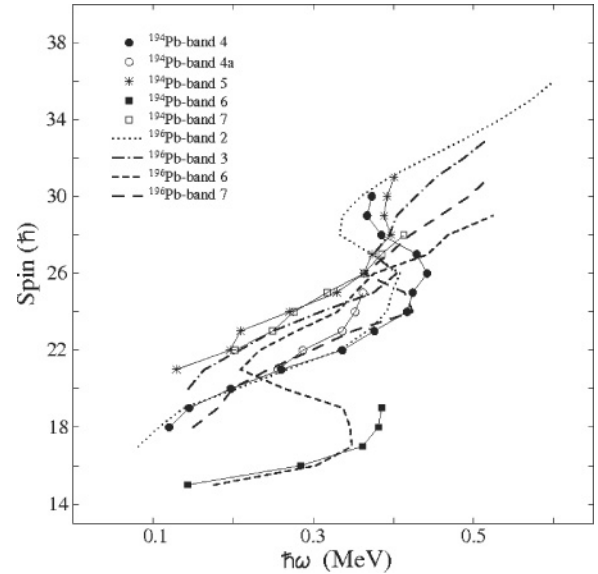
has been assigned to band 4 (band 1a in Ref. [19]) and a CD alignment is suggested in the upbend region [19]. The same configurations are assigned to band 2 in ^{196}Pb [18] and band 3 in ^{198}Pb [30]. It is seen in Fig. 8 that band 4 in ^{194}Pb seems to gain the same alignment of $\sim 7.5\hbar$ at a crossing frequency $\hbar\omega = 0.4$ MeV, which is slightly higher than that of band 2 in ^{196}Pb. Thus the configurations AB11 and ABCD11 can be confirmed for band 4 at low and high spin, respectively. Band 5 contains the two level sequences 1b and 1c of Ref. [19] but it starts at much higher excitation energy and spin in our work. This definitely rules out the assignment given to band 1b in Ref. [19] as a four-proton excitation resulting from a coupling of a $(\pi h_{11/2})^2$ excitation to the proton 11^- state. Band 5 shows regular level spacings and no $E2$ crossover transitions were observed, which is a behavior typical for a magnetic band. It decays into band 4 below the crossing with the AB11 configuration. From Fig. 8 it can be seen that the alignment of band 5 is about $2.5\hbar$ higher than that of band 4. Similar bands were also observed in ^{196}Pb (band 3 [18]) and in ^{198}Pb (band 2 [30]). Based on their excitation energy and spin the configuration ABEF11 was proposed for them [18,30]. We also accept the configuration ABEF11 for band 5. The alignment behavior in the crossing region is different for the ABEF11 bands in ^{194}Pb and ^{196}Pb (see Fig. 8). Band 3 in ^{196}Pb has smaller alignment gain at slightly higher rotational frequency than the CD crossing observed for AB11 band 2. An alignment of the next neutron $i_{13/2}$ pair is proposed [18] and band 3 is assigned configuration ABEFGH11 at high spin. In ^{198}Pb the corresponding band 2 experiences band crossing at the same rotational frequency as band AB11 and an alignment of CD neutrons is proposed [30]. As a result, the configuration ABCDEF11 is suggested above the band crossing in ^{198}Pb [30]. However, the alignment is not completed and the gain is not defined. The initial alignment of band 5 in ^{194}Pb is higher than that of band 3 in ^{196}Pb but the total alignment gain may be larger than the one of a GH pair.

We prefer, therefore, the configuration ABCDEF11 for band 5 above the crossing.

TAC model calculations performed for the negative-parity configurations [18] predict that the AE8 configuration should be excited at the lowest spin. We observed a new magnetic band, named band 6, with $I^\pi = 14^-$ bandhead at an energy of 4264.6 keV, which we suggest to be the AE8 band. A similar band (band 6 in Ref. [18]) with a bandhead also at spin 14^- and at energy 4385 keV was observed in ^{196}Pb [18].

Band 7 was previously observed in Ref. [19] as their band 4 and assigned an ABCE8 configuration. Band 7 might be a continuation of the newly observed band 6. One may speculate that the exact connection could not be observed because it is very weak. Indeed, in Fig. 8, a comparison of bands 6 and 7 with band 6 in ^{196}Pb [18] reveals a strong resemblance. The configurations of AE8 and ABCE8 were proposed for band 6 in ^{196}Pb [18] before and above the band crossing, respectively. Thus, we tentatively suggest the configuration ABCE8 for band 7. However, the possibility that band 7 is not a continuation of band 6 is quite possible and cannot be ruled out.

The short new sequence, band 4a, decays into the AB11 band 4. Its initial alignment is close to that of band 4 and lower than that of ABEF11 band 5 (see Fig. 8). The structure of band 4a is probably close to that of band 4. TAC calculations performed in Ref. [18] predict that the configuration AC11 is one of the first three energetically favored configurations. The configurations AC11/ACEF11 were proposed for band 7 in ^{196}Pb [18]. This band has not been connected to lower lying states. The decay pattern and the initial alignment of band 4a would better fit the AC11 configuration before the upbend. However, we could not observe lower lying levels and because the alignment is not completed (Fig. 8) it is not possible to draw any definite conclusions about the nature of the aligning pair.

V. SUMMARY

The level scheme of ^{194}Pb has been investigated by the ^{30}Si $+$ ^{168}Er reaction by using the Euroball III multidetector array. The many new structures that were added to the normal states allowed us to correct the excitation energies and spins of previously observed MR bands. Four new bands of $M1$ transitions were found and some levels have been reordered, resulting in new sequences. Only one new band could not be connected to the lower lying states. Based on these experimental results and on systematic comparison with neighboring ^{196}Pb and ^{198}Pb isotopes, reliable configuration assignments were made to the well-developed dipole bands. The nucleus ^{194}Pb was found to follow closely the systematics of heavier Pb isotopes. In this mass region the magnetic rotational bands are described as high-j particle-hole $2p$-$2n$ configurations. In the normal part of the level scheme states of pure neutron, intruder proton, and mixed proton-neutron character could be identified. This part of the level scheme may provide an important material for detailed theoretical investigation, which may answer some fundamental questions about the behavior of this nucleus as well as its neighbors.

ACKNOWLEDGMENTS

[1] W. Nazarewicz, Phys. Lett. **B305**, 195 (1993).
[2] B. Singh, R. Zywina, and R. B. Firestone, Nucl. Data Sheets **97**, 241 (2002).
[3] A. Lopez-Martens *et al.*, Eur. Phys. J. A **20**, 49 (2004).
[4] A. N. Wilson *et al.*, Phys. Rev. Lett. **95**, 182501 (2005).
[5] K. Vyvey, G. D. Dracoulis, A. N. Wilson, P. M. Davidson, A. E. Stuchbery, G. J. Lane, A. P. Byrne, and T. Kibédi, Phys. Rev. C **69**, 064318 (2004).
[6] G. D. Dracoulis, G. J. Lane, T. M. Peaty, A. P. Byrne, A. M. Baxter, P. M. Davidson, A. N. Wilson, T. Kibedi, and F. R. Xu, Phys. Rev. C **72**, 064319 (2005).
[7] M. Ionescu-Bujor *et al.*, Phys. Lett. **B650**, 141 (2007).
[8] G. Baldsiefen *et al.*, Nucl. Phys. **A574**, 521 (1994).
[9] S. Frauendorf, Nucl. Phys. **A557**, 259c (1993).
[10] A. Singh *et al.*, Phys. Rev. C **66**, 064314 (2002).
[11] S. Frauendorf, Z. Phys. A **358**, 163 (1997).
[12] A. O. Macchiavelli, R. M. Clark, P. Fallon, M. A. Deleplanque, R. M. Diamond, R. Krucken, I. Y. Lee, F. S. Stephens, S. Asztalos, and K. Vetter, Phys. Rev. C **57**, R1073 (1998).
[13] A. O. Macchiavelli, R. M. Clark, M. A. Deleplanque, R. M. Diamond, P. Fallon, I. Y. Lee, F. S. Stephens, and K. Vetter, Phys. Rev. C **58**, R621 (1998).
[14] A. O. Macchiavelli, R. M. Clark, M. A. Deleplanque, R. M. Diamond, P. Fallon, I. Y. Lee, F. S. Stephens, and K. Vetter, Phys. Rev. C **58**, 3746 (1998).
[15] A. O. Macchiavelli, R. M. Clark, M. A. Deleplanque, R. M. Diamond, P. Fallon, I. Y. Lee, F. S. Stephens, and K. Vetter, Phys. Lett. **B450**, 1 (1999).
[16] Amita, A. K. Jain, and B. Singh, At. Data Nucl. Data Tables **74**, 283 (2000).
[17] H. Hübel, Prog. Part. Nucl. Phys. **54**, 1 (2005).
[18] A. Singh *et al.*, Nucl. Phys. **A707**, 3 (2002).
[19] M. Kaci *et al.*, Nucl. Phys. **A697**, 3 (2002).
[20] J. Simpson, Z. Phys. A **358**, 139 (1997).
[21] D. Radford, Nucl. Instrum. Methods Phys. Res. A **361**, 297 (1995).
[22] B. Fant *et al.*, J. Phys. G **17**, 319 (1991).
[23] D. Mehta *et al.*, Z. Phys. A **345**, 169 (1993).
[24] M.-G. Porquet *et al.*, J. Phys. G **20**, 765 (1994).
[25] N. Sandulescu, A. Insolia, B. Fant, J. Blomqvist, and R. Liotta, Phys. Lett. **B288**, 235 (1992).
[26] C. Pomar, J. Blomqvist, R. Liotta, and A. Insolia, Nucl. Phys. **A515**, 381 (1990).
[27] P. Duppen, M. Huyse, and J. L. Wood, J. Phys. G **16**, 441 (1990).
[28] K. Heyde, J. Jolie, J. Moreau, J. Ryckebusch, M. Waroquier, P. Duppen, M. Huyse, and J. L. Wood, Nucl. Phys. **A466**, 189 (1987).
[29] R. Bengtsson and W. Nazarewicz, Z. Phys. A **334**, 269 (1989).
[30] A. Görgen *et al.*, Nucl. Phys. **A683**, 108 (2001).